Autocorrelation Techniques in Color Flow Imaging: Signal Model and Statistical Properties of the Autocorrelation Estimates

Hans Torp, *Member, IEEE*, Kjell Kristoffersen, and Bjørn A. J. Angelsen, *Senior Member, IEEE*

***Abstract*—A review of the scattering theory for moving blood, and a model for the signal in a multigated pulsed wave Doppler system is presented. The model describes the relation between a general time-variable velocity field and the signal correlation in space and time, including the effect of movement of the ultrasonic beam for color flow imaging systems with mechanical scanning. In the case of a constant and rectilinear velocity field, a parametric model for the autocorrelation function is deduced. General formulas for a full second order characterization of the set of autocorrelation estimates, with arbitrary lags in the spatial and temporal directions, are developed. The formulas are applied to the parametric model, and numerical results for the estimator variance are presented. A qualitative evaluation of the theoretical results has been performed by offline-processing of 2-D Doppler signals from a color flow imaging scanner. The benefit of spatial and temporal averaging is demonstrated by using different averaging filters to the same set of recorded data.**

NOMENCLATURE

$k_o = \omega_o/c$	Wave number
$v(\underline{r}, t)$	Velocity field as a function of space r and time t.
(r, Υ, ϕ)	Spherical coordinates with center in the transducer rotation-center and scanning plane in $\phi = 0$.
$(v_r, rv_\Upsilon, rv_\phi)$	Spherical components of the velocity field.
$s(r)$	Radial range gate function
T	Pulse repetition time interval.
$\Upsilon_(\underline{r}, t)$	Blood cell fluctuation, spectral density.
$\zeta(\underline{r}, t, \tau)$	Displacement of a fluid element during time τ
ζ_r	Radial component of the displacement ζ.
Δ	Distance between the range gates in the radial direction.
L	Radial length of the sample volume.
T_r	Radial transit time.
T_Υ	Lateral transit time.
T_ϕ	Transversal transit time.
Ω	Transducer rotation angular velocity.
f_d	Doppler frequency shift
$\omega_d = 2\pi T f_d$	Normalized angular Doppler frequency shift
$\otimes$	Convolution operator
$R(n, m)$	Autocorrelation function for the Doppler signal with lag n in radial direction, and lag m in temporal direction.
$\mathbf{R}(n, m)$	Autocorrelation *estimate* of $R(n, m)$.
$\phi(n, m)$	Phase of the complex autocorrelation estimate $\mathbf{R}(n, m)$
$c(n, m)$	2-D smoothing filter coefficients.
$C_*(n_1, m_1, n_2, m_2)$	Covariance between $\mathbf{R}(n_1, m_1)^*$ and $\mathbf{R}(n_2, m_2)$
$C(n_1, m_1, n_2, m_2)$	Covariance between $\mathbf{R}(n_1, m_1)$ and $\mathbf{R}(n_2, m_2)$

Manuscript received July 1, 1993; revised March 14, 1994; accepted March 16, 1994. This work was supported by the Norwegian Research Council.

H. Torp and B. A. J. Angelsen are with the Department of Biomedical Engineering, Medical Technical Center, N-7005 Trondheim, Norway.

K. Kristoffersen is with Vingmend Sound Research Department, Vollsveien 13C, N-1324 Lysaker, Norway.

IEEE Log Number 9403352.

I. INTRODUCTION

AUTOCORRELATION TECHNIQUES for two-dimensional (2-D) velocity imaging were first developed for weather Radar applications [1], and later applied to blood velocity imaging [2]. Originally, each range cell along the beam was processed individually, to estimate the signal parameters. More recently algorithms using data from several range cells have been presented [3], [4]. In this case the movement of the blood between the range cells has an influence on the statistical properties of the estimates. It is therefore convenient to model the received signal as a 2-D complex Gaussian process, described by an autocorrelation function with lag in both the radial (along the beam), and the temporal directions. For color flow imaging with a mechanical sector scan, the movement of the ultrasonic beam over the sector must be taken into account. This movement causes rapid changes in the signal properties as the beam sweeps over different flow-patterns in the body. To maintain spatial resolution, only a small number of signal samples can be used for calculation of the blood flow parameters at each point of the sector, giving autocorrelation estimates with a high fractional variance.

A number of authors have modeled the Doppler signal from moving blood as a zero-mean Gaussian process, with power spectrum equal to a blurred version of the velocity distribution inside the sample volume [5]–[7]. To justify the Gaussian assumption, the received signal is modeled as a sum of independent signal components from a large number of point-scatterers, each contributing a slightly modified replica

of the transmitted pulse, with a delay according to the distance from the transducer. In [4] a scattering model for blood is given, based on a random continuum model for the red blood cell distribution, which leads to an expression for the autocorrelation function of the received signal. The random continuum approach has also been used in a recent work of Mo *et al.* [8] to characterize the power spectrum in continuous wave Doppler. Bonnefous *et al.* [3] describe the cross correlation between the consecutive received RF signals in a color flow mapping system due to the movement of the red blood cells. Ferrara *et al.* [4], describe the received signal as a one-dimensional (1-D) complex Gaussian process, and show how the autocorrelation function for a uniform velocity field is nearly periodic, with period close to the pulse repetition time. In [9] their model is extended to account for frequency dependent scattering and attenuation.

This paper is organized as follows. In Section II and III, the autocorrelation function for the signal is described for a general velocity field, based on the random continuum scattering model for moving blood. Section IV describes the rectilinear flow situation, where the magnitude of the complex autocorrelation function gets a Gaussian form, described by three parameters. Section V contains general formulas for the covariance of the set of autocorrelation estimates. These results are applied to the parametric model in Section VI. Experimental results with color flow images, showing the benefit of radial averaging, are presented in Section VII.

II. Transient Pulse Echo Response from Blood

The signal model presented in this paper is based on a random continuum model for the scattering from blood [10]. The spatial fluctuations in mass density and compressibility, which determine the incoherent part of the scattering, are assumed to be proportional to the spatial fluctuation in the red blood cell concentration $n_b(\underline{r}, t)$, where $\underline{r}$ is spatial position, and t is time. The fluctuation function is defined as the difference between the actual cell concentration and its local average. Thus $n_b(\underline{r}, t)$ is a zero-mean, random process in space and time. Assuming a short correlation in space for a fixed time t, and neglecting diffusion, the autocorrelation function for $n_b(\underline{r}, t)$ is approximated as [10]

$$\langle n_b(\underline{r}, t) n_b(\underline{r} + \underline{\xi}, t + \tau) \rangle = \Upsilon(\underline{r}, t) \quad \delta(\underline{\xi} - \underline{\zeta}(\underline{r}, t, \tau))$$
$$\Upsilon(\underline{r}, t) = \frac{\text{var}\,(n_b(\underline{r}, t) \cdot \Delta V)}{\Delta V} \tag{1}$$

where $\underline{\zeta}(\underline{r}, t, \tau)$ is the displacement of the fluid element in position $\underline{r}$ during the time interval t to $t + \tau$. The function $\Upsilon(\underline{r}, t)$ is the variance per unit volume in the number of blood cells inside a small volume ΔV, and this quantity is proportional to the backscattering coefficient from blood. For stationary velocity fields, the function $\Upsilon(\underline{r}, t)$ as well as the displacement function will be independent of time t. In this case, the process $n_b(\underline{r}, t)$ is stationary in time. If in addition the velocity field is rectilinear and uniform, and the quantity γ is constant in space, the process $n_b(\underline{r}, t)$ will be stationary in both space and time.

The point scatterer response $e(t, \underline{r})$ is defined as the electrical response in the receiver from a point scatterer in position $\underline{r}$ when the transducer is excited with an electrical pulse at time $t = 0$. The waveform as well as the amplitude of the point scatterer response $e(t, \underline{r})$ are influenced both by the aperture geometry, and by the frequency dependent attenuation and scattering of the insonified medium. To obtain the signal from blood, the point scatterer response is multiplied with the cell concentration function at the time when the transmitted pulse arrives at the point $\underline{r}$, and the product is integrated over space.

$$y(t) = \int d^3 r e(t, \underline{r}) n_b\left(\underline{r}, t - \frac{r}{c}\right) \tag{2}$$

Here c is the speed of sound and $r = |\underline{r}|$ is the distance from the origin, which is in the center of the transducer. The round-trip time for the echo is $t = \frac{2r}{c}$. The blood velocity is much lower than the speed of sound, so it is reasonable to neglect the movement of the blood cells during the short time when the pulse transverses the blood sample. This means that $n_b(\underline{r}, t - \frac{r}{c}) \approx n_b(\underline{r}, t/2)$ in (2). Both the waveform and the amplitude of the point scatterer response $e(t, \underline{r})$ will vary with the spatial position of the scatterer. In a region near the beam axis and the focal point, the received waveform will be close to a replica of the transmitted waveform, whereas in the sidelobes of the beam, the received waveform will have a longer, and more irregular shape [11].

The spatial variation of the point scatterer response amplitude depends to some extent on the transmitted pulse wave form. For continuous wave excitation, the beam profile in the far field has a form close to a sinc function with one main lobe and periodical side lobes [12]. For the short pulse excitation, the main lobe has almost the same shape, while the side lobes are smeared out [11]. The excitation waveform most commonly used in ultrasound Doppler is a wave burst with a rectangular envelope. The resulting beam profile will consequently be something in-between the two extreme cases, continuous wave, and delta pulse excitation, depending on the pulse length.

The following example shows that the contribution from the side lobes in the ultrasonic beam can be neglected. Suppose that the transducer insonates a large blood vessel, so that the entire beam, including the side lobes resides inside the blood vessel. The contribution to the power of the Doppler signal from a small volume element of blood in position $\underline{r}$ is proportional to the 4th power of the ultrasonic pressure amplitude in $\underline{r}$, assuming that the same transducer is used for transmit and receive. The volume elements will behave like independent scatterers due to the short correlation distance in the blood cell fluctuation. For a transducer with a circular symmetric beam profile $E(r_0)$, where r_0 is the distance from the beam axis, the contribution to the signal power from a cylindrical volume around the beam axis, with radius R is found by integration, using cylindrical coordinates (r_0, ϕ)

$$P(R) \sim \int_{|r_0|<R} dr_0 d\phi \; r_0 \; E(r_0)^4 = \int_0^R dr_0 \; 2\pi r_0 E(r_0)^4 \tag{3}$$

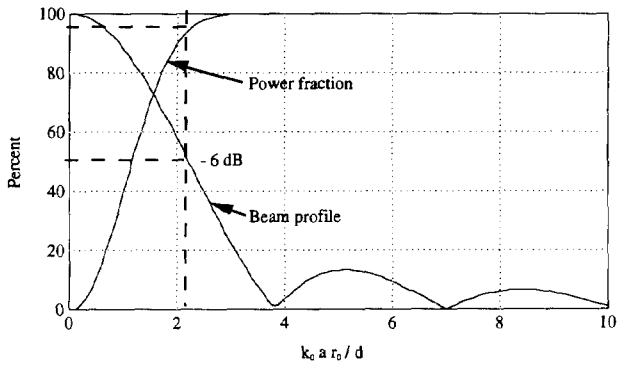

Fig. 1. The beam profile in the far field from a circular disk transducer of radius a, and the power fraction form a cylindrical region around the beam center axis, as a function of distance r_0 from the axis. The horizontal axis is scaled in the dimensionless parameter $k_0 a r_0/d$, where k_0 is the wavenumber, and d is the distance from the transducer.

In Fig. 1 the one-way beam profile $E(R)$, and the corresponding fractional power contribution $P(R)/P(\infty)$ are plotted as a function of the distance R from the beam center axis. Observe that with this beam profile, which is the far-field approximation of a plane, circular disk transducer, 94% of the power comes from the region inside the -6 dB beam opening angle.

The axial variation of the point scatterer response waveform will still be significant, caused by aperture geometry and frequency dependent attenuation and scattering. This variation will be slow compared to the pulselength, so that locally, the point scatterer response can be separated in a normalized pulse waveform $p(t)e^{i\omega_0 t}$, and a spatial sensitivity function $B(\underline{r})$. After quadrature demodulation, the complex Doppler signal takes on the form

$$x(t) = \int d^3r B(r) p \otimes h\left(t - 2\frac{r}{c}\right) \cdot e^{2ik_0 r} n_b(r, t/2) + n_0 \otimes h(t) \quad (4)$$

Two way beam-profile amplitude:	$B(r)$
Complex envelope of the point scatterer response:	$p(t)$
Receiver lowpass filter impulse response:	$h(t)$
Wavenumber for the received signal center frequency:	$k_0 = \omega_0/c$
Thermal additive noise:	$n_0(t)$

Note that the pulse waveform p will change with the elapsed time t after transmission, due to frequency dependent attenuation. The noise $n_0(t)$ is assumed to be white, and independent of the signal. The temporal variation of the blood cell fluctuation $n_b(\underline{r}, t/2)$ is assumed to be slow, compared to the speed of sound, and is therefore not affected by the receiver filter.

III. Autocorrelation Function for the Received Signal

Assume that the transducer is excited with a series of pulses, with repetition time interval T. The received signal from the mth pulse is (neglecting contribution from previous pulses)

$$x_m(t) = \int d^3r B_m(\underline{r}) e^{2ikr} p \otimes h\left(t - 2\frac{r}{c}\right) n_b(\underline{r}, mT + t/2) + n_0 \otimes h(mT + t) \quad (5)$$

To account the movement of the beam in mechanical scanner systems, the transducers spatial sensitivity function is indexed with the pulse number $B_m(\underline{r})$. The convolution of the transmitted pulse and the receiver filter impulse response determines the radial extension of the sample volume, and is denoted $s(\frac{1}{2}ct) \equiv p \otimes h(t)$. Note that s is in general complex valued, but for symmetrical spectrum around ω_0, this function will be real valued. In a practical system, the signal is sampled in the continuous time parameter t, which corresponds to the radial position $r = ct/2$. After sampling with radial increments Δ, the signal can be described by a 2-D complex Gaussian matrix $x(n, m) = x_m(\frac{2n\Delta}{c})$, with a joint probability density function defined in terms of the autocorrelation function with lag n in radial, and m in temporal direction.

$$R(n, m; n_0, m_0) = \langle x(n_0, m_0)^* \cdot x(n_0 + n, m_0 + m) \rangle \quad (6)$$

The expression for the autocorrelation of the red blood cell concentration in (1) is now used to derive an expression for $R(n, m; n_0, m_0)$, valid for a general velocity field. Note that the blood cell concentration is assumed to be delta-correlated in space.

$$R(n, m; n_0, m_0) = \int d^3\underline{r} B_{m_0}(\underline{r}) B_{m_0+m}(\underline{r} + \underline{\zeta}) s(r - n_0\Delta)^* \times s(r + \zeta_r - (n_0 + n)\Delta) \Upsilon(\underline{r}, m_0 T) e^{2ik_0\zeta_r} + N_0 h_2\left(2\frac{n\Delta}{c}\right)\delta(m')$$
$$\underline{\zeta} = \underline{\zeta}(\underline{r}, m_0 T + r/c, mT) \quad (7)$$

The entity ζ_r is the component of the displacement function $\underline{\zeta}$ in the radial direction. The receiver noise component is independent of the signal from blood, causing the cross-correlation term to disappear. N_0 is the noise power, and the function h_2 is the autocorrelation integration operator applied to the receiver filter impulse response

$$h_2(t) \equiv \int du\, h(u)\, h(u + t) \quad (8)$$

When the flow velocity field is locally rectilinear and constant (i.e., within the size of the sample volume), the displacement function $\underline{\zeta}(\underline{r}, t, \tau) \approx \underline{v}(\underline{r}, t)\tau$, and the phase $2k_0\zeta_r$ relates directly to the radial velocity component v_r.

IV. A Parametric Model for the Autocorrelation Function in Regions With Locally Rectilinear Blood Flow

The general expression for the autocorrelation function given in (7) is not very useful for quantitative evaluation of color flow imaging algorithms. To obtain a reasonably simple model, blood flow regions with a constant rectilinear velocity

field in space and time is considered. The scattering cross section per unit volume blood $\Upsilon(\underline{r})$ is also assumed to be constant in this region. It is convenient to use spherical coordinates $\underline{r} = (r, \Upsilon, \phi)$ with origin in the transducer rotation center, and scanning plane in $\phi = 0$. The velocity is decomposed into spherical components $\underline{v} = (v_r, rv_\Upsilon, rv_\phi)$, where v_Υ and v_ϕ are angular velocities in the lateral (in the scan plane) and the transversal direction, respectively. The displacement function $\underline{\zeta}$ can then be written $\underline{\zeta} = (v_r mT, v_\Upsilon mT, v_\phi mT)$, and the red cell fluctuation function $n_b(\underline{r}, t)$ will then be stationary, both in space and time. To make the integrand of (7) separable in (r, Υ, ϕ), some further assumptions are done:

1) Only regions where $s(r - n_0\Delta)$ is different from zero contribute to the volume integral. The function $s(r)$ is the convolution between the transmitted pulse, and the receiver filter response, which is limited to a few wavelengths. In this small sample volume, the spatial sensitivity function $B(\underline{r})$ for the transducer is assumed to be constant in the radial direction.
2) It is assumed that the transversal variation of B can be separated in Υ and ϕ. This is motivated from the Gaussian shape of the function B.
3) The analysis is restricted to regions where the ultrasonic beam has a fixed or continuously moving angular position, with a constant angular rotation speed Ω. For phased array and linear array systems, $\Omega = 0$.

With these assumptions, the spatial sensitivity function is separable in the lateral and the transversal direction, and takes on the form

$$B_{m_0}(\underline{r}) \sim \Psi(\Upsilon - \Omega mT)\ \Phi(\phi) \tag{9}$$

The functions Ψ, Φ, and s will in general depend on the sample volume depth $n\Delta$, but the variation is slow, and it can be neglected over the range where the autocorrelation is nonzero. With these assumptions the integral in (7) can be separated in (r, Υ, ϕ) as follows:

$$\begin{aligned} R(n, m; n_0, m_0) = \int & r^2 d\underline{r} s^*(r - n_0\Delta) \\ & s(r + v_r mT - (n_0 + n)\Delta) e^{2ikv_r mT} \\ & \cdot \int d\Upsilon \Psi(\Upsilon - \Omega m_0 T) \\ & \cdot \Psi(\Upsilon - \Omega(m_0 + m)T + v_\Upsilon mT) \\ & \cdot \int d\phi \Phi(\phi)\Phi(\phi + v_\phi mT) \end{aligned} \tag{10}$$

The term r^2 will be almost constant $= (n_0\Delta)^2$ within the sample volume. Each of the three integrals now has the form of a convolution, and can therefore be expressed in a more compact way (up to a scaling factor, dependent on $n_0\Delta$).

$$\begin{aligned} R(n, m; n_0, m_0) = s_2(v_r mT - n\Delta) \cdot \Psi_2(\Omega m + v_\Upsilon mT) \cdot \\ \Phi_2(v_\phi mT) \cdot e^{2ikv_r mT} \end{aligned} \tag{11}$$

The subscript 2 for the functions s, Ψ, and Φ is a notational convention for the autocorrelation integral operator, as defined in (8). In this form, the magnitude of the complex autocorrelation function is factorized in three "transit time functions", defining the correlation length in radial, lateral, and transversal direction. The phase factor accounts for the Doppler shift due to the radial velocity component v_r in the blood flow. Note that this autocorrelation model is invariant in space and time.

In a mechanical scanning system with a circular transducer, the functions Ψ and Φ are equal, and may be found as the square of the pressure wave transversal beam profile. All of the three functions s, Ψ, and Φ have a symmetrical shape around the maximum value, and they are almost monotonically decreasing. The autocorrelation of such functions has a shape close to the Gaussian, i.e., $f(x) = \exp(-x^2)$.

In practical implementations, both the transmitted pulse envelope and the receiver filter impulse response are often designed with rectangular shapes. This receiver filter was shown in [13] to give a nearly optimum trade off between radial resolution, and SNR, provided that the impulse response is equal to the pulse length. The pulse response after receiver filter $s(r)$, is then equal to $f_T(\frac{r}{L})$, where L is the pulse length, and f_T is the triangular function given by

$$f_T(x) = \begin{cases} 1 - |x| & \text{for} |x| < 1 \\ 0 & \text{for} |x| \geq 1 \end{cases} \tag{12}$$

The second moment of the function $f_T \otimes f_T(r/L)$ equals $\frac{L^2}{3}$, giving the Gaussian approximation $e^{-3r^2/(2L^2)}$. It is now possible to give a simple description of these functions, with a model containing two parameters; the transmitted pulse length L, and the beam opening angle Θ.

$$\begin{aligned} s_2(r) = f_T \otimes f_T\Big(\frac{r}{L}\Big) \approx e^{-\frac{3r^2}{2L^2}}, \quad L = \text{ pulse length} \\ \Psi_2(\nu) = \Phi_2(\nu) \approx e^{-\frac{3\nu^2}{2\Theta}}, \quad \Theta = \text{ beam opening angle} \end{aligned} \tag{13}$$

The parameter Θ corresponds to the -3.25 dB beam opening angle, both for a Gaussian beamprofile, and for the far-field approximation field for a circular plane disk transducer. It is convenient to define the *transit time* in radial, lateral, and transversal direction T_r, T_Υ, T_ϕ as the time the scatterers use to travel a distance L, and angle Θ, respectively. The time unit is T, the pulse repetition time.

$$\begin{aligned} T_r &= \frac{L}{v_r T} \\ T_\Upsilon &= \frac{\Theta}{(v_\Upsilon - \Omega)T} \\ T_\phi &= \frac{\Theta}{v_\phi T} \end{aligned} \tag{14}$$

The transducer rotation speed Ω is taken into account by subtracting it from the lateral velocity component. It is also convenient to introduce the *normalized Doppler frequency shift* ω_d, which is the phase shift between two adjacent pulses due to the radial velocity component $v_r, \omega_d = 2kv_r T$.

By combining the (11), (13), and (14), the autocorrelation function gets the form of a 2-D Gaussian probability density function in (n, m)

$$\begin{aligned} R(n, m) &= R(0, 0)\beta(n, m)e^{i\omega_d m} \\ \beta(n, m) &= e^{-\frac{1}{2}Q(n,m)} \end{aligned}$$

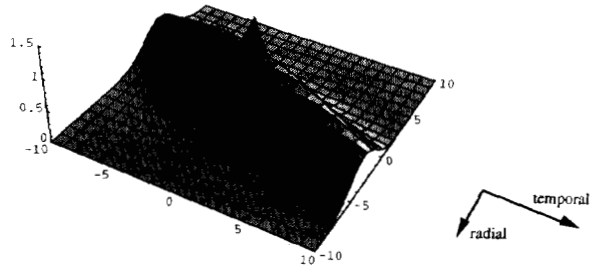

Fig. 2. A plot of the magnitude of the complex 2-D autocorrelation function $R(n, m)$ as a function of temporal lag m, and radial lag n.

$$Q(n,m) = \left(\frac{n}{\sigma_1}\right)^2 + 2\rho\frac{n}{\sigma_1}\frac{m}{\sigma_2} + \left(\frac{m}{\sigma_2}\right)^2 \tag{15}$$

The parameters σ_1, σ_2, and ρ for the quadratic form $Q(n,m)$ are given by

$$\begin{aligned}\sigma_1 &= \frac{L}{\sqrt{3}\Delta} \\ \rho &= \frac{T_r^{-1}}{\sqrt{\frac{1}{T_r^2} + \frac{1}{T_\Upsilon^2} + \frac{1}{T_\phi^2}}} \\ \sigma_2 &= \rho\frac{T_r}{\sqrt{3}}\end{aligned} \tag{16}$$

These three parameters have the following physical interpretation: σ_1 and σ_2 are the correlation lengths in radial and temporal direction, whereas the crosscorrelation coefficient ρ shows to what extent the same fluid elements remain inside the volume insonified by the ultrasonic beam. If the lateral velocity component follows the beam movement, the same blood cells will be observed in several range cells; T_Υ and T_ϕ then become large compared to T_r, and ρ will be close to unity. An example which shows a typical shape of $|R(n,m)|$ is presented in Fig. 2. The flow direction is purely radial, and a receiver noise component of -6 dB, relative to the signal power makes a discontinuity in $n = 0, m = 0$.

V. Second-Order Statistics for the Autocorrelation Estimates

The estimates of the autocorrelation function considered in this work are a weighted mean of product terms of the signal $x(n,m)$ in the neighborhood of the point (n_0, m_0) with weighting coefficients $c(l,k)$

$$\begin{aligned}R(n,m;n_0,m_0) = \sum_l \sum_k c(l,k)x^*(n_0+l, m_0+k) \\ \times x(n_0+l+n, m_0+k+m)\end{aligned} \tag{17}$$

The process $x(n,m)$ is assumed to be *locally* stationary, i.e., the true autocorrelation function is constant in the region where $c(l,k) \neq 0$. To simplify the notation, n_0 and m_0 are set to 0 in the following, and omitted from the expressions. The correlation estimate is unbiased, provided that the sum of the coefficients in the averaging filter equals unity. In order to deduce all the covariance elements between the real and imaginary parts in the complex matrix $\{\mathbf{R}(n,m)\}_{n,m}$, both $\mathrm{Cov}(\mathbf{R}^*(n_1,m_1), \mathbf{R}(n_2,m_2))$, and $\mathrm{Cov}(\mathbf{R}(n_1,m_1), \mathbf{R}(n_2,m_2))$ for any combination of (n_1, m_1, n_2, m_2) are needed. In the subsequent part of this paper the following short-notation for the covariance will be used:

$$\begin{aligned}C_*(n_1,n_2,m_1,m_2) &\equiv \mathrm{Cov}(\mathbf{R}^*(n_1,m_1), \mathbf{R}(n_2,m_2)) \\ C(n_1,n_2,m_1,m_2) &\equiv \mathrm{Cov}(\mathbf{R}(n_1,m_1), \mathbf{R}(n_2,m_2))\end{aligned} \tag{18}$$

These covariance values can be expressed by the true autocorrelation function, by applying the "factoring of moment"—properties for complex Gaussian processes [14, p. 601]. Details can be found in the appendix.

$$\begin{aligned}&C_*(n_1,n_2,m_1,m_2) \\ &\quad = \sum_{kl} c_2(l,k)R(l,k)R^*(l+n_1-n_2, k+m_1-m_2) \\ &C(n_1,n_2,m_1,m_2) \\ &\quad = \sum_{kl} c_2(l,k)R(l+n_1,k+m_1)R^*(l-n_2,k-m_2) \\ &c_2(l,k) = \sum_{k_1 l_1} c(l_1,k_1)c(l_1+l,k_1+k)\end{aligned} \tag{19}$$

Higher order moments can be deduced in a similar way. Note that the complex valued autocorrelation estimates do not constitute a set of jointly complex Gaussian variables, as defined in [15, p. 77]. From the first equation in (19) it follows that the variance of $|\mathbf{R}(n,m)|$, which is the sum of variance in the real and the imaginar part of $\mathbf{R}(n,m)$, are identical for all lags (n,m).

$$\begin{aligned}\mathrm{Var}(|R(n,m)|) &= C_*(n,n,m,m) \\ &= \sum_{kl} c_2(l,k)|R(l,k)|^2\end{aligned} \tag{20}$$

In practical implementations, an averaging filter with a rectangular impulse response is often used, i.e., $c(n,m) = \frac{1}{N}\frac{1}{M}$, with length N in the radial direction, and M in the temporal direction. The funtion c_2 in (19) then takes on the form of a product of two triangular functions [defined in (12)]

$$c_2(n,m) = \frac{1}{N}\frac{1}{M} f_T\left(\frac{n}{N}\right) f_T\left(\frac{m}{M}\right) \tag{21}$$

If the correlation length of the signal is short compared to the averaging filter size, the function $c_2(l,k)$ is nearly constant, and equal to $c_2(0,0)$ in the area where $R(l,k)$ is nonzero. This is a 2-D version of the "strong filtering approximation" described in [16], where the covariance is proprtional to the equivalent noise bandwidth (ENBW) of the averaging filter

$$\mathrm{ENBW} = c_2(0,0) = \sum_{k_1 l_1} c(l_1,k_1)^2 \tag{22}$$

For the rectangular averaging filter, the equivalent noise bandwidth equals the inverse of the number of nonzero filter coefficients, $\mathrm{ENBW} = \frac{1}{MN}$.

The argument (phase angle) of the autocorrelation estimate $\phi(n,m) = \arg(\mathbf{R}(n,m))$, denoted *correlation angle estimator*, may serve as a mean frequency estimator. Most commonly used is the correlation angle estimator with lag $n = 0, m = 1$, but algorithms combining $\phi(0,m)$ from several lags m have been proposed, and their properties have been studied by simulations [17]. When the fractional variance of $\mathbf{R}(n,m)$ is

small, the covariance between the correlation angle estimators with different lags has an approximate expression given by the first and second order moments of $\{\mathbf{R}(n,m)\}$, see appendix.

$$\begin{aligned}&\operatorname{covar}\{\phi(n_1,m_1),\phi(n_2,m_2)\}\\&\approx\frac{1}{2}\operatorname{Re}\left\{\frac{C_*(n_1,n_2,m_1,m_2)}{R(n_1,m_1)^*R(n_2,m_2)}-\frac{C(n_1,n_2,m_1,m_2)}{R(n_1,m_1)R(n_2,m_2)}\right\}\end{aligned}\tag{23}$$

This result is a straight forward generalization of the variance expression in [1, eq. A3].

VI. Covariance Expressions Applied to the Parametric Signal Model

The general covariance expressions in the previous section will now be developed further for the parametric model presented in Section IV. By inserting (15) in (19), it turns out that the two covariance expressions can be expressed by a common function denoted $\mathrm{CS}(n,m)$.

$$\begin{aligned}&C_*(n_1,n_2,m_1,m_2)\\&\quad=S^2\beta(n_1-n_2,m_1-m_2)e^{-i\omega_d(m_1-m_2)}\\&\qquad\times\mathrm{CS}(n_1-n_2,m_1-m_2)\\&C(n_1,n_2,m_1,m_2)=S^2\beta(n_1,m_1)\beta(n_2,m_2)e^{i\omega_d(m_1+m_2)}\\&\qquad\times\mathrm{CS}(n_1-n_2,m_1-m_2)\\&\mathrm{CS}(n,m)\\&\quad=\sum_{kl}c_2(l,k)\beta(l,k)^2\\&\qquad\times\exp\left(\frac{n}{\sigma_1}\left(\frac{1}{\sigma_1}+\rho\frac{k}{\sigma_2}\right)+\frac{m}{\sigma_2}\left(\rho\frac{1}{\sigma_1}+\frac{k}{\sigma_2}\right)\right)\end{aligned}\tag{24}$$

The approximate expression for the covariance of the correlation angle estimators, (23) applied to the parametric model yield:

$$\begin{aligned}&\operatorname{covar}\{\phi(n_1,m_1),\phi(n_2,m_2)\}\\&\approx\frac{1}{2}\left\{\frac{\beta(n_1-n_2,m_1-m_2)}{\beta(n_1,m_1)\beta(n_2,m_2)}-1\right\}\mathrm{CS}(n_1-n_2,m_1-m_2)\\&\operatorname{var}\{\phi(n,m)\}\approx\frac{1}{2}\left(\beta(n,m)^{-1}-1\right)\mathrm{CS}(0,0):|m|>0\end{aligned}\tag{25}$$

This result shows that the minimum variance of $\phi(n,m)$ is obtained when $\beta(n,m)$ attains its maximum value, i.e. when the autocorrelation magnitude has its maximum. Depending on the radial velocity component, this maximum may occur at nonzero radial lag n, see Fig. 2. The variance is also proportional to CS(0, 0), which equals the fractional variance of the signal power estimate $\mathbf{R}(0,0)$.

$$\mathrm{CS}(0,0)=\sum_{kl}c_2(l,k)\beta(l,k)^2\approx c_2(0,0)\sum_{kl}\beta(l,k)^2\tag{26}$$

The latter form of CS(0, 0) is the strong filtering approximation described in the previous section. In Fig. 3 the fractional variance in its exact form, and the strong filtering approximation are compared for different averaging filters. Parameter values in the model are selected to match the experimental data presented in the next section; these are $L=\Delta, T_r=T_\Upsilon=8$. The averaging filter is rectangular,

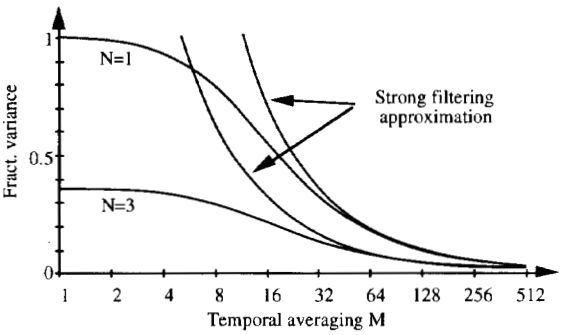

Fig. 3. Fractional variance of the autocorrelation estimates as a function of lateral averaging, for two different values of radial averaging; $N=1$, and $N=3$. Strong filtering approximation, compared with the exact expression (25).

with a temporal averaging M varying from 1 to 512 points, and the radial averaging lengths $N=1$ and $N=3$. Note that radial averaging reduces the variance more rapidly than temporal averaging. The strong filtering approximation shows a large over-estimation of the estimator variance when the filter length M is less than 32, which is four times the temporal correlation length.

VII. Experiments and Discussion

A. Instrumentation and Signal Processing

The ultrasound recordings were made with a mechanical color flow sector scanner (CFM700, Vingmed Sound, Horten, Norway). Doppler quadrature components from 64 range gates with 12 bit resolution were collected in real-time and transferred via a custom data grabber unit to an external computer. The stored Doppler signals were separately high-pass filtered for each range-gate to remove clutter echoes. Autocorrelation estimates for zero and unity lags, $\mathbf{R}(0,0)$ and $\mathbf{R}(0,1)$, were calculated using rectangular averaging filters both in the radial and temporal directions, and signal power P, center frequency ω, and bandwidth b were calculated by [16]

$$\begin{aligned}P&=10\log(\mathbf{R}(0,0))\\\omega&=\arg(\mathbf{R}(0,1))\\b&=\sqrt{1-\frac{|\mathbf{R}(0,1)|}{\mathbf{R}(0,0)}}\end{aligned}\tag{27}$$

Note that the variance of $\mathbf{P}$ and ω both are proportional to the variance parameter CS(0, 0), (26). The signal power is used to determine areas in the image where moving blood is present, whereas the bandwidth is used as a "disturbed flow" indicator. High bandwidth is caused by high velocities, giving short transit time, or large velocity gradients within the sample volume. Two different color coding schemes were used to map these parameter estimates in a 2-D display.

1) Power/frequency map: The color intensity was modulated with log-compressed signal power, whereas the center frequency determined the color hue, in a continuous rainbow-scale over the values $0<\omega<2\pi$.
2) Bandwidth/frequency map: The center frequency was mapped in a red-violet-blue color scale for low

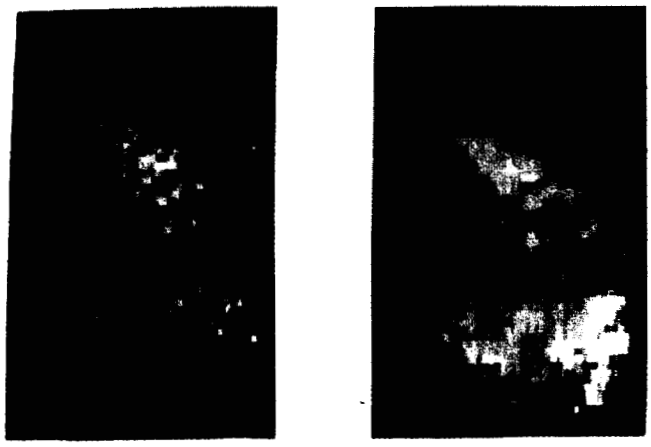

Fig. 4. The problem of "dropouts" in a color flow image showing mitral flow into the left ventricle. To the left: No radial averaging filter. To the right: 3 point radial averaging.

bandwidth, gradually changing to uniformly green as the bandwidth increased. The signal power was tested against a threshold to remove noise from the image.

B. Results and Discussion

In this subsection, some examples with 2-D Doppler data recorded from the left ventricle of the human heart are shown, with emphasis on comparing different averaging filters for the autocorrelation estimates to the same data.

The initial experiments with color flow imaging showed that the variance of the *signal power estimate* degraded the image quality, especially when the SNR was poor. The effects were "dropouts", and poor border definition of the flow regions. This is illustrated in Fig. 4, left panel, which shows mitral blood flow into the left ventricle of the human heart in early diastole. A 16 point temporal averaging filter is used for the autocorrelation estimates. In the right panel the same data is used, but with additional 3 point radial averaging. The improved performance with the 3 point radial averaging filter illustrates the theoretical values for the variance reduction shown in Fig. 3.

An important clinical application of color flow imaging is to detect the position and size of valvular leakage in the human heart. Fig. 5 shows color flow images from a patient with an aortic valve leakage, with and without 3 point radial averaging filter. The aortic valve regurgitant jet with the base in the lower left part of the image creates a region of disturbance in the blood velocity field of the left ventricle. The bandwidth estimates along the indicated horizontal line in the images are shown as a green curve in the lower part in each of the images. The three point radial averaging filter (shown to the right), reduces the variance of the bandwidth estimate, thus giving a more sharp outline of the disturbed flow region.

Fig. 6 shows a sequence of four consecutive images through the cardiac cycle from the same patient. Upper 4 images are without radial averaging, and lower 4 images are with 3 point radial averaging. The first three images show the filling of the left ventricle, and the development of the aortic regurgitant jet flow. The last image is in systole, with aortic outflow to the

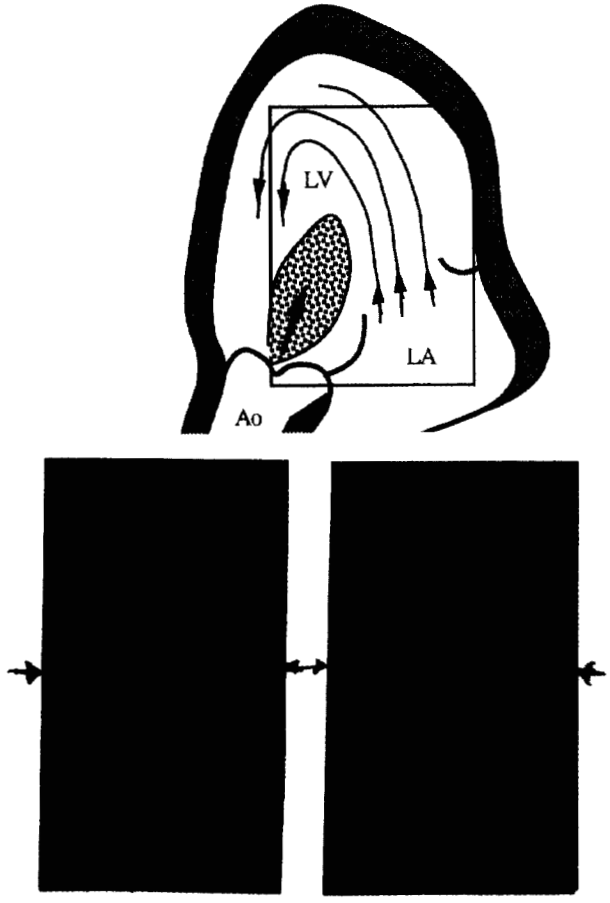

Fig. 5. Aortic insufficiency jet mixing with regular mitral inflow. The green curve below shows the bandwidth estimate along a horizontal line across the jet area. To the left: No radial averaging filter. To the right: 3 point radial averaging.

right, and a small mitral valve insufficiency jet to the lower right. Upper sequence is with and without radial averaging. Fig. 7 shows a summary of the effect of different averaging filter sizes, both in time and range, applied to the same data, where one gets an impression of the trade off between spatial resolution, and smoothness of the image.

VIII. Conclusion

The signal model for a general nonstationary blood-velocity field was based on the assumption of locally invariant point scatterer response waveform. This was justified by showing that only the main lobe in the ultrasonic beam contributes to the Doppler signal. The autocorrelation function was expressed as a volume integral of the local scattering cross section with a phase factor given by the radial displacement of the scatterers. This corresponds to a result in [10], slightly generalized. For stationary and rectilinear flow, the magnitude of the 2-D complex autocorrelation function was shown to have a Gaussian form, described by three velocity dependent transit-time parameters. Frequency dependent scattering and attenuation may modify both the bandwidth and the center frequency of the received signal. This can be taken into account by adjusting the mixing frequency ω_0 and the sample volume length L in the model.

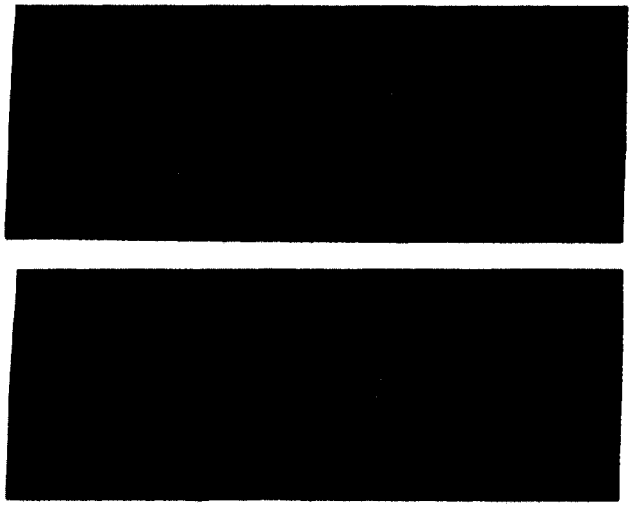

Fig. 6. The improvement obtained by radial averaging shown on a sequence of color flow images with a large aortic regurgitation and a small mitral insufficiency (rightmost image). Lower sequence: No radial averaging filter. Upper sequence: 3 point radial averaging.

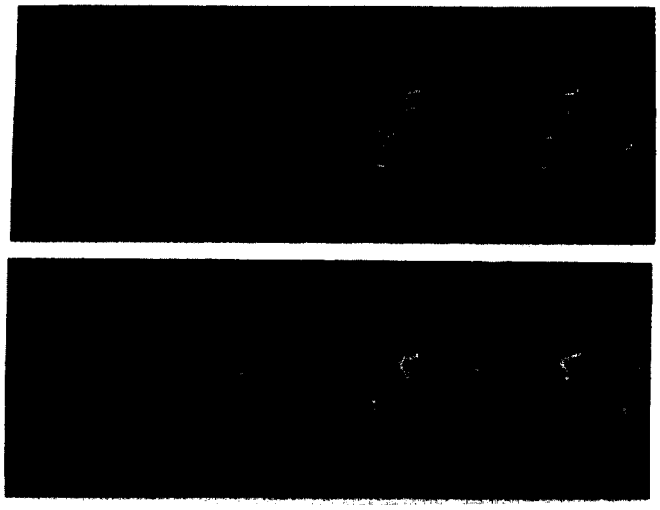

Fig. 7. Eight different averaging filters applied to the same data as in Fig. 5. Temporal averaging are 4, 8, 16, and 32, increasing from left to right. Radial averaging is 1 point (upper row) and 3 point (lower row).

The general covariance expressions in Section IV show that the variance of the autocorrelation function *magnitude* estimate is constant for all lags, and equal to the variance of the signal power estimate. For the parametric model the variance of the real part, imaginary part, as well as the phase angle of the autocorrelation estimate for any lag were proportional to the fractional variance of the signal power estimate. Numerical calculations for the fractional variance using the parametric model, show that the "strong filtering approximation" where the covariance is proportional to the equivalent noise bandwidth of the averaging filter, is not accurate for typical averaging filters used in color flow imaging.

Improvements in the mean frequency estimator are possible to achieve by using correlation estimates with nonzero lag in the radial direction. However, significant improvements can only be obtained for high velocities.

The experimental part demonstrates the impact of the averaging filter on the image quality in color flow imaging. For the examples shown, the radial averaging increases the quality, with little loss in resolution. The theoretical results predict a 60% reduction in variance of signal power and mean frequency estimates, when radial averaging is applied. This was not verified quantitatively with the experimental data; however, it was clearly demonstrated that radial averaging is more efficient than temporal averaging. Variance and bias of the bandwidth estimator has previously been analyzed by Zrnić [18] and Kristoffersen [16]. Their results are based on low fractional variance of the autocorrelation estimate. Since this assumption is seldom satisfied in color flow imaging, no attemt is done here to generalize these results to 2-D processes.

APPENDIX

A. General Covariance Expressions

Covariance of the correlation function estimates of real-valued Gaussian processes is treated in several textbook, e.g., [19]. It seems likely that similar expressions for complex, zero mean Gaussian processes exist in the open literature, but the authors of this paper have not been able to find adequate references. The formulas are developed here, in a similar way as for the real case.

The correlation between estimates with two different sets of lags can be expressed as a sum of fourth-order moments by applying the definition in (17)

$$\begin{aligned}&\langle R^*(n_1,m_1)R(n_2,m_2)\rangle \\ &\quad=\sum_{l_1k_1}\sum_{l_2k_2}c(l_1,k_1)c(l_2,k_2)\langle x(l_1,k_1)\\ &\qquad x^*(l_1+m_1,k_1+m_1)x^*(l_2,k_2)x(l_2+n_2,k_2+m_2)\rangle\end{aligned} \tag{A1}$$

Assume that y_1, y_2, y_3, and y_4 are joint complex Gaussian random variables, the forth order moments can factorized into second order moments, see [14, pp. 601] or [20]:

$$\langle {y_1}^* y_2 {y_3}^* y_4\rangle = \langle {y_1}^* y_2\rangle\langle {y_3}^* y_4\rangle + \langle {y_1}^* y_4\rangle\langle {y_3}^* y_2\rangle \tag{A2}$$

Note that this expression contains one product term less than the corresponding formula for real Gaussian variables. This result is combined with (A1) to express the covariance by the true autocorrelation function $\mathbf{R}(n,m)$.

$$\begin{aligned}\langle \mathbf{R}^*(n_1,m_1)\ \mathbf{R}(n_2,m_2)\rangle &= R^*(n_1,m_1)\ R(n_2,m_2)\\ &+\sum_{l_1k_1}\sum_{l_2k_2}c(l_1,k_1)c(l_2,k_2)\ R(l_1-l_2,k_1-k_2)\\ &\times R^*(l_1-l_2+n_1-n_2,k_1-k_2+m_1-m_2)\end{aligned} \tag{A3}$$

The last term in this equation is the covariance between $\mathbf{R}^*(n_1,m_1)$ and $\mathbf{R}(n_2,m_2)$. The double sum in (A3) can be rearranged, giving the final form in (19)

$$\begin{aligned}&\mathrm{Cov}(\mathbf{R}^*(n_1,m_1),\mathbf{R}(n_2,m_2))\\ &\quad=\sum_{kl}\left(\sum_{k_1l_1}c(l_1,k_1)c(l_1-l,k_1-k)\right)R(l,k)\end{aligned}$$

$$\times R^*(l+n_1-n_2, k+m_1-m_2)$$
$$= \sum_{kl} c_2(l,k) \quad R(l,k)$$
$$\times R^*(l+n_1-n_2, k+m_1-m_2) \qquad \text{(A4)}$$

The expression for $\mathrm{Cov}(\mathbf{R}(n_1,m_1),\mathbf{R}(n_2,m_2))$ can be deduced in a similar way.

B. Covariance of the Correlation Phase Angle Estimates

If z_1 and z_2 are two complex random variables with low fractional variances, then the covariance between the phase angles $\phi_1 = \arg(z_1)$ and $\phi_2 = \arg(z_2)$ is approximately equal to

$$\mathrm{cov}(\phi_1,\phi_2) \approx \frac{1}{2}\mathrm{re}\left\{\frac{\langle z_1 z_2^*\rangle}{\langle z_1\rangle\langle z_2^*\rangle} - \frac{\langle z_1 z_2\rangle}{\langle z_1\rangle\langle z_2\rangle}\right\} \qquad \text{(A5)}$$

This relation is applied with $z_1 = \mathbf{R}(n_1,m_1)$, and $z_2 = \mathbf{R}(n_2,m_2)$, which gives (23).

ACKNOWLEDGMENT

The authors would like to thank A. Heimdal and X. Lai of the Department of Biomedical Engineering for their help in searching for literature and fruitful discussions.

REFERENCES

[1] D. S. Zrnić, "Spectral moment estimates from correlated pulsed pair," *IEEE Trans. Aerosp. Electron.*, vol. AES-13, pp. 344–354, 1977.
[2] C. Kasai, K. Namekawa, A. Koyano, and R. Omoto, "Real-time two-dimensional blood flow imaging using an autocorrelation technique," *IEEE Trans. Sonics Ultrason.*, vol. SU-32, pp. 458–464, 1985.
[3] O. Bonnefous and P. Pesqué, "Time domain formulation of pulse-doppler ultrasound and blood velocity estimation by cross-correlation," *Ultrason. Imaging*, vol. 8, pp. 73–85, 1986.
[4] X. Ferrara and X. Algazi, "A new wideband spread target maximum likelihood estimator for blood velocity estimation—Part I: Theory," *IEEE Trans. Ultrason., Ferroelec., Freq. Contr.*, vol. 38, pp. 1–26, 1991.
[5] W. R. Brody and J. D. Meindl, "Theoretical analysis of the CW Doppler ultrasonic flowmeter," *IEEE Trans. Biomed. Eng.*, vol. BME-21, pp. 183–192, 1974.
[6] B. A. J. Angelsen and K. Kristoffersen, "On ultrasonic MTI measurement of velocity profiles in blood flow," *IEEE Trans. Biomed. Eng.*, vol. BME-26, pp. 665–671, 1979.
[7] V. L. Newhouse, P. J. Bendick and L. W. Varner, "Analysis of transit time effects on Doppler flow measurements," *IEEE Trans. Biomed. Eng.*, vol. BME-23, pp. 381–387, 1976.
[8] L. Y. L. Mo and R. S. C. Cobbold, "A unified approach to modeling the backscattered doppler ultrasound from blood," *IEEE Trans. Biomed. Eng.*, vol. 39, pp. 450–461, 1992.
[9] X. Ferrara and X. Algazi, "The effect of frequency dependent scattering and attenuation on the estimation of blood velocity using ultrasound," *IEEE Trans. Ultrason., Ferroelec., Freq. Contr.*, vol. 39, pp. 754–767, 1992.
[10] B. A. J. Angelsen, "A theoretical study of the scattering of ultrasound from blood," *IEEE Trans. Biomed. Eng.*, vol. BME-27, pp. 61–67, 1980.
[11] M. A. Fink and J. F. Cardoso, "Diffraction effects in pulse-echo measurement," *IEEE Trans. Sonics Ultrason.*, vol. SU-31, pp. 313–329, 1984.
[12] P. M. Morse and K. U. Ingard, *Theoretical Acoustics*. New York: McGraw-Hill, 1968.
[13] K. Kristoffersen, "Optimal receiver filtering in pulsed doppler ultrasound blood velocity measurement," *IEEE Trans. Ultrason., Ferroelec., Freq. Contr.*, vol. UFFC-33., pp. 51–58, 1986.
[14] H. L. van Trees, *Detection, Estimation, and Modulation Theory, Part III*. New York: Wiley, 1971.
[15] K. Miller, *Complex Stocastic Processes*. Reading, MA: Addison-Wesley, 1974.
[16] K. Kristoffersen, "Time domain estimation of the center frequency and spread of doppler spectra in doppler ultrasound," *IEEE Trans. Ultrason., Ferroelec., Freq. Contr.*, vol. 35, pp. 484–497, 1988.
[17] P. R. Mahapatra and D. S. Zrnić, "Practical algorithms for mean velocity estimation in pulsed doppler weather radars using a small numbers of samples," *IEEE Trans. Geosci. and Remote Sensing*, vol. GE-21, pp. 491–501, 1983.
[18] D. S. Zrnić, "Spectrum width estimates for weather echoes," *IEEE Trans. Aerosp. Electron.*, vol. AES-15, pp. 613–619, 1979.
[19] G. Jenkins and D. Watts, "Spectral Analysis and its Applications," Holden-Day, 1968.
[20] J. L. Doob, *Stochastic Processes*. New York: Wiley, 1953.

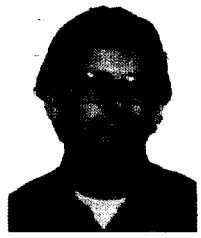

Hans G. Torp (M'92) was born in Sarpsborg, Norway, in 1953. He received the M.S. and Dr.Techn. degrees from the University of Trondheim, Norway, in 1978 and 1992, respectively.

From 1979 to 1983 he was with the Division of Automatic Control, SINTEF (The foundation of Scientific and Industrial Research), Trondheim. Since 1983 he has been working with the Department of Biomedical Engineering, Faculty of Medicine, University of Trondheim. He is currently a research Fellow, holding a stipend from the Norwegian Research Council. His research areas includes stochastic signal/image processing with applications in ultrasonic imaging, Doppler and color flow imaging.

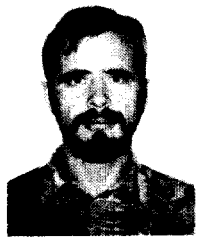

Kjell Kristoffersen was born in Karmøy, Norway, in 1952. He received the M.S. and Dr. Techn. degrees from the Norwegian Institute of Technology, Trondheim, Norway in 1978 and 1986, respectively.

From 1978 to 1984 he worked with research and development in several areas of process identification and Doppler ultrasound at the Division of Automatic Control, SINTEF, Trondheim, Norway. Since 1984 he has been involved with development of medical ultrasound imaging systems at Vingmed Sound A.S., where he currently holds the position as Director of Research. His research interests include signal processing with application to medical imaging and noninvasive diagnosis.

Bjørn A. J. Angelsen (M'79-SM'82) was born in Vestvågøy, Norway, in 1946. He received the M.S. and Dr.Techn. degrees from the Norwegian Institute of Technology, Trondheim, Norway, in 1971 and 1977, respectively.

From 1971 to 1972 he worked on infrared detectors at the Norwegian Defence Research Establishment, Kjeller, Norway. From 1972 to 1975 he held a stipend at the Norwegian Institute of Technology and from 1975 to 1982 he was with the Division of Control Engineering, SINTEF, The Foundation of Scientific and Industrial Research, Norwegian Institute of Technology, Trondheim, Norway. From 1977 to 1978 he was on leave at the Department of Electrical Engineering, University of California, Berkeley, and the Division of Biomedical Engineering, Stanford Research Institute, Menlo Park, CA. Since 1980 he has been Adjunct Professor of Biocybernetics and since 1983 a Professor of Biomedical Engineering at the University of Trondheim. His research interests include noninvasive diagnosis with emphasis on ultrasonic diagnosis.